RSC Advances

Polymer Functionalized Magnetic Nanoconstructs for Immunomagnetic Separation of Analyte

Journal:	*RSC Advances*
Manuscript ID	RA-ART-06-2016-014236.R1
Article Type:	Paper
Date Submitted by the Author:	01-Jul-2016
Complete List of Authors:	Chattopadhyay, Sruti; Indian Institute of Technology Delhi, Centre for Biomedical Engineering Kaur, Avneet; Indian Institute of Technology Delhi, Centre for Biomadical Engineering Jain, Swati; Indian Institute of Technology Delhi (IIT D), Center for Biomedical Engineering Sabharwal, Prabhot; Indian Institute of Technology Delhi, Centre for Biomedical Engineering Singh, Harpal; IIT Delhi, Biomedical Engg; IIT, CBME
Subject area & keyword:	Biomedical < Biological

Polymer Functionalized Magnetic Nanoconstructs for Immunomagnetic Separation of Analyte

Sruti Chattopadhyay*, Avneet Kaur, Swati Jain, Prabhjot K. Sabharwal and Harpal Singh*

Centre for Biomedical Engineering, Indian Institute of Technology-Delhi, N.D.-16, India

Abstract

Magnetic nanoparticles are promising materials for immunomagnetic separation of various proteinaceous and genetic entities, and are used in the field of biosensing. In this paper, we have reported synthesis and evaluation of novel terpolymeric functionalized magnetic nanoconstructs (PFMNCs) as an effective immunomagnetic separator and sensing platform. Multistep strategy was adopted to prepare the functionalized magnetic nanoconstructs. Iron oxide dispersion was synthesized by coprecipitation method followed by stabilization using sodium oleate as surfactant (IONPs). Finally, encapsulation of preformed IONPs was done by in-situ emulsion polymerization of styrene, methyl methacrylate and acetoacetoxy ethyl methacrylate in presence of varied amounts (3-21% w/w) of surfactant stabilized IONPs. Nanoconstructs were characterized by spectral, morphological and various analytical techniques. Polymeric nanoconstructs with 6% IONPs exhibited good dispersion stability, superparamagnetic properties and well defined core shell morphology with 123 nm magnetic core and 54 nm shell thickness. PFMNCs were evaluated as an immunomagnetic matrix for the detection of analyte by sandwich ELISA. Amino groups of antibodies (GAR-IgG) were covalently attached to pendant di-ketonic functionalities of nanoconstructs with high immobilization efficiency of 85%. Polymeric magnetic nanoconstructs can efficiently separate the target entities from the aqueous solution, which leads to the lower detection limit of 0.39 ng/mL of analyte, RAG-IgG. The developed nanoconstructs demonstrate

dual capabilities of working as an immunomatrix as well as magnetic separator and thus have a strong potential for the use in clinical diagnostics.

---

sruticiitd@gmail.com

avneetvincle@hotmail.com

swatijain.iitd@gmail.com

prabsabharwal@hotmail.com

Corresponding Authors: *harpal2000@yahoo.com, *sruticiitd@gmail.com

Keywords

Iron oxide nanoparticles, polymeric nanoconstructs, immobilization, immunomagnetic separation, antibodies, detection

Abbreviations

Iron oxide IO

Nanoparticles NPs

Polymer functionalized magnetic nanoconstructs PFMNCs

Sodium oleate NaOA

AAEM Acetoacetoxy ethyl methacrylate

1. Introduction

The current decade had seen the emergence of functionalized magnetic nanoparticles in rapidly advancing technologies pertaining to drug delivery, hyperthermia treatment of cancerous growth, MRI contrast enhancement methods and in clinical diagnosis. Magnetic systems provide improved and convenient mechanism for delivering payloads and separating biological species from a milieu of products. Immunomagnetic separation is a pre-concentration method widely used in biomedicine, food safety and environmental monitoring primarily for sample enrichment, cleanups and manipulations. Magnetic particles/beads are an integral part for ensuring immunological separation of components coupled with various biosensing techniques to improve efficiency and reduce the time of analysis.[1,2]

Magnetic iron oxide nanoparticles (IONPs) have large surface to volume ratio and consequently have high surface energy which is spontaneously stabilized by aggregation process favoring entropy and free energy criteria. Stability of naked IONPs is poor at neutral pH of water and physiological fluids resulting in quick precipitation and aggregation during the synthesis or upon storage. Their high chemical activity makes them susceptible for oxidation, which results lowering in magnetism and dispersion ability[3]. Therefore, steric as well as electrostatic stabilization is required to ensure dispersibility in aqueous medium. A protective impermeable coating of secondary material seems a straightforward answer to solve this problem. Generally, low molecular weight surface ligands are used to anchor or physically adsorb on multilayered organization and create repulsive forces on NPs which in turn stabilize the dispersion by inhibiting particulate aggregation[4,5].

Multifaceted polymers have become popular for passivating and activating IONPs owing to their advantage of easy tunability to get desirable properties by altering surface characteristics such as

hydrophilicity, functionality, charges etc. These magnetoresponsive polymeric entities inherit unique combinatorial properties of both components: polymers and magnetic nanoparticles. Magnetically stimulated polymeric beads provide instant actions and can be controlled via remote systems without any direct contact while retaining easy processability of polymeric network. Various bio-inspired, bioactive natural and synthetic polymers are applied for creating different morphologies such as core-shell and nanospheres where either magnetic core is surrounded by polymer shell of varied thickness or magnetic particles are homogenously distributed inside the polymer beads respectively. Polymers provide surface ligating functional groups enabling receptors or catalysts to bind with biomolecules. Chitosan, dextran, polyvinyl alcohol, polyethylene glycols, polylactic acid and alginates based assembly have been created for capping iron oxide nanoparticles in the last few years.[6-9] However, recent studies reveal that surface inhomogeneity of these coatings resulted in non-specific adsorption of proteins posing roadblock in both therapeutic and diagnostic applications.[10]

Butt et al[11] have created a novel nematicidal platform of polymer-brush grafted magnetic nanoparticles for the immobilization of specific protease enzyme (from *Streptomyces griseus*). They have used multistep process such as generation of silica coated amino functionalized magnetic nanoparticles followed by oxidative ATRP to yield poly(glycidyl methacrylate) brushes on magnetic nanoparticles. Polymer brush based protease functionalized MNPs showed higher enzyme activity as compared to the free enzyme. However many of the proposed reactions, which operate on multiple chemistries, enhance processing time as well as complexities.

In another article molecularly imprinted polymer core–shell superparamagnetic nanoparticles have been prepared by surface-mediated RAFT polymerization of thin dimethylacrylamide and *N*,*N*′-

methylene(bis)acrylamide layers on oleic acid-stabilized iron oxide nanoparticles. The composite nanoparticle of 20 nm dimension was obtained and showed specific molecular recognition of cholesterol.[12] Dai et al[13] have coated super hydrophilic poly(2-methacryloyloxyethyl phosphorylcholine polymer on magnetic nanoparticles demonstrating superior capture efficiency of *Salmonella* from raw milk by PCR than natural dextran coated nanoparticles. Most of these protocols involve multiple reaction steps involving either numerous derivatizations or require sophisticated monomeric compounds for the subsequent generation of functional groups on the surface of composite nanosystem. In addition, for many of them further functionalization is necessary for coupling with biomolecules. Disuccinimidylsuberate (DSS)[14], Protein A[15], polyguanine (polyG) oligonucleotide[16] are some of the linkers used for attaching biomolecules on magnetic nanomaterials.

In this paper we report preparation of acetoacetoxy functionalized terpolymeric nanoconstructs with magnetic stimulus for immunomagnetic separation of analytes. Emulsion polymerization of acrylic monomers, with different polarity, was carried out to obtain polymeric nanoconstructs encapsulating different amounts of magnetic nanoparticles. Diketonic functionalities on the surface of nanoconstructs were exploited for the direct immobilization of biomoleucles without using any linker or catalyst. Developed magnetic nanoconstructs were evaluated for the separation and detection of biomolecules using GAR-IgG and RAG-IgG as a model system.

2. Experimental Section

2.1 Materials

Analytical grades of ferrous chloride ($FeCl_2.4H_2O$), ferric chloride ($FeCl_3.6H_2O$), aqueous ammonium hydroxide (25%), styrene (St), methyl methacrylate (MMA) and sodium

peroxydisulphate (SPDS), ammonium persulphate (APS) were purchased from CDH Chemicals (Mumbai, India). Sodium oleate (NaOA) with 99% purity and acetoacetoxyethylmethacrylate (AAEM) were from Sigma Aldrich (NJ, USA). Styrene and MMA were purified by conventional method using (0.1M) sodium hydroxide to remove hydroquinone from the monomers and distilled at reduced pressure. All other chemicals were used as received unless noted otherwise. Immunoreagents - Goat anti-rabbit (GAR) and rabbit anti-goat (RAG) immunoglobulins (IgGs), enzyme conjugate GAR-HRP (horse raddish peroxidase) and ELISA substrate 3, 3′, 5, 5′tetra methyl benzidine/hydrogen peroxide (TMB/H_2O_2) solution were all purchased from Bangalore Genie (Bangalore, India). De-ionized MilliQ water (18Ω, Millipore, India) was used in all experiments for preparation of nanoparticles and requisite buffers.

2.2 Synthesis of modified iron oxide nanoparticles

Co-precipitation method was followed for the synthesis of IONPs. Two separate solutions of $FeCl_3.6H_2O$ and $FeCl_2.4H_2O$ were mixed under nitrogen blanket with continuous stirring. The total iron content was kept constant at 7.0 g with 2:1 molar ratio of Fe III:II chlorides. 42 mL of 25% ammonium hydroxide was added dropwise and the reaction was stirred for 30 minutes to obtain black coloured solution. This iron oxide precipitate was collected by applying external magnetic field and washed with 0.1 (N) hydrochloric acid followed by distilled water for several times to remove acid residues while maintaining the pH around 7-8. Oleate treatment was performed using the published procedure with some modifications. Briefly, 90mg of sodium oleate in 10 mL of water was incorporated to 300 mg (70 mg/mL) aqueous dispersion of IO precipitate in a RB flask maintaining 1:1 molar ratio. The mixture was heated at 80°C for 10 mins with constant stirring under nitrogen atmosphere and then sonicated for another 10 mins. The black colored surfactant

coated nanoparticles,termed as IONPs in rest of the paper, were directly introduced in the polymerization flask.

2.3 Synthesis of PFMNCs

Polymer coated magnetic nanoparticles were prepared by free radical emulsion polymerization with addition of reactants in two steps. A 250 mL RB flask was equipped with mechanical stirrer, reflux condenser, thermometer, dropping funnel and nitrogen purging unit for the subsequent removal of inhibitor oxygen. Calculated amounts of IONPs varying from 3-21% w/w of total monomer concentration were dispersed in 80 mL of distilled water by ultrasonication for 10 mins and transferred to RB flask. A homogenous solution of 1.75 mL styrene, 0.5 mL MMA and 0.5 mL AAEM was added to the magnetic dispersion and emulsion was heated to 60°C for 15 mins. Aqueous initiator solution of SPDS (80 mg/mL) was mixed into the system and the seeding polymerization step was continued for 2 h at 80°C. Afterwards emulsion temperature was reduced to 40°C and second lot of monomers was introduced. 1.25 mL St, 0.5 mL MMA, 0.3 mL AAEM along with mixed initiator system of SPDS and APS (80 mg/mL each) were added. Temperature was further increased to 80°C and stirring was continued for 8 h for the complete polymerization of monomers. Different nanoconstructs were designated according to the percentage of incorporated IONPs and are termed as PFMNC-3, 6, 9, 12, 15 and 21 for 3%, 6%, 9%, 12%, 15% and 21% IONPS respectively. The nanoconstructs were lyophilized and reserved for the next step of bio-immobilization.

2.4 Characterization of PFMNCs

Generation of different functional groups on the surface of nanosystem during sequential synthesis steps was monitored by Attenuated Total Reflectance–Fourier Transform infrared (ATR-FTIR) spectroscopy (Perkin Elmer Spectrum One spectrometer, USA) measurements with scanning wavelengths from 400 to 4000 cm^{-1}. Particle size and structure of IO and polymeric nanoconstructs were evaluated by transmission electron microscope (TEM, TECNAI, FEI, USA). 5 μL of dilute aqueous magnetic dispersions were placed on 200 mesh Cu grid and air dried for few mins to maintain a very thin coating of sample and the grid was fed inside the instrument chamber at 27°C operating at 200kV. Scanning electron microscopy (SEM) images were acquired by EVO (ZEISS EVO series, EVO 50, UK) for assessing the surface morphology. Lyophilized nanoparticles were mounted on a round metallic stub using a double sided tape. They were further coated with a thin micrometric layer of gold by spin coater (Bio-Rad Polaran Sputter, Model 50X) to enhance the resolution of images. X-Ray diffraction pattern of IONPs and PFMNCs was recorded with a Philips X'Pert PRO Thin Film X-ray Diffractometer (USA) at wavelength Cu-K_α= 1.5406Å operating at current of 40 mA and voltage of 45 kV at the rate of 2°/min in Bragg-Bretano geometry in 2θ range of 20-80°. XRD peaks were indexed according to ICCD data collection and compared with magnetite standards. Magnetic content in PFMNCs were assessed by thermal gravimetric assay (TGA, TA instruments Q-500, USA) under nitrogen atmosphere at a heating rate of 20°C/min in a temperature range of 30° to 600°C using Al cups. Lyophilized samples were used for the same.

Size of modified NPs was evaluated along with size distribution and zeta potential by Zeta Sizer, Nanoseries Dynamic Light Scattering Instrument (Malvern Instruments Ltd., Nano ZS90, USA). The data for each measurement was collected for 10 runs with 10 cycles per run using 50 mV laser and KCl solution as calibrating agent. The magnetic properties of IONPs and nanoconstructs were

measured by Super Conducting Quantum Interference Device (SQUID, Quantum Design Ever Cool, USA). The analysis was done at 300K by sweeping the magnetic field from -6T to +6T (KOe) to attain optimal magnetic saturation (Ms) values. Effect of pH (5-8) on the magnetic property of nanoconstructs was also studied.

2.5 Immobilization of Abs

PFMNCs were evaluated as solid matrix for immobilization of specific biomolecules for their eventual application as nano-sized sequestration and biosensing agent. 3mg of optimized PFMNC-6 were incubated with different dilutions of (1:2000-1:64000) GRA-HRP conjugate at 4°C for 16h. Afterwards PFMNC-GAR-HRP were magnetically isolated from the remaining medium by placing the eppendroffs on a 1T permanent magnet for 30 sec and the washing was done with 1X-PBS buffer three times. After removal of unbound conjugate, the activity of immobilized HRP was evaluated using chromogenic conversion of TBM/H_2O_2 substrate in10 mins. 100 µL of this solution was strategically transferred in different wells of microtitre plate and further 'stop' reagent H_2SO_4 (0.5M) was added to quench the reaction. Signal measurement of nanoconstruct-enzyme conjugate PFMNC-GAR-HRP was done using ELISA plate reader (BioTek, Epoch, USA) at 450 nm wavelength. Amount of immobilized GAR-Ab on synthesized PFMNCs and immobilization efficiency were estimated by Pierce® BCA Protein Assay kit. Nanoconstructs were immobilized with 500 µl of the optimized concentration of GAR-Ab (1 µg/ mL). Amount of the antibody immobilized on PFMNCs was determined by calculating the initial and final concentration of Ab in the immobilization solution.

2.6 Immunomagnetic separation and colourimetric detection of Abs

A prototype of immunomagnetic separation and biosensing approach was proposed with PFMNCs which performed dual role of separating agent and immobilization support. PFMNCs were incubated with 500 µL (1µg/mL) of primary GAR-Ab for 16 h at 4°C and are designated as PFMNC-GAR. 6% skimmed milk was further added to immobilized nanoconstructs to block unreacted sites. Corresponding complementary RAG-Ab was taken as the analyte in the procedure and primary Ab attached PFMNC-GAR were incubated with fixed concentration of 500 µL of 50 ng/mL of the analyte. This was followed by incubation with 500 µLof enzyme conjugate of the primary antibody, GAR-HRP. After removal of unbound conjugate, signal measurement of PFMNC-GAR-RAG-GAR-HRP was done by using TBM/H_2O_2 substrate as described in above section 2.5. In the negative control PFMNC-GAR were incubated with 500 µL of 1X-PBS buffer instead of RAG-IgG in the assay procedure and the same protocol was followed as mentioned above. The data are mentioned as NSB (nonspecific binding of primary antibody) in the graph. All incubations were done at 37° C for 1 h in incubator shaker and washing was performed after every incubation step three times each with Tween/PBS and 1X-PBS.

3. Results and Discussion

A multistep approach was employed for the synthesis of polymer functionalized magnetic nanoconstructs as an effective immunomagnetic nanobeads for the immobilization of biomolecules. Firstly, iron oxide dispersion was stabilized with optimal concentration of surfactant followed by encapsulation within polymeric network. Miniemulsion polymerization was performed with a combination of three monomers in presence of different amounts of iron oxide nanoparticles. This resulted in the formation of polymeric nanoconstructs of various sizes having an inherent surface active acetoactoxy functionality for the attachment specific Abs.

Synthesis of IONPs

Co-precipitation method was adopted for the preparation of iron oxide particles in aqueous medium under alkaline conditions yielding black precipitate which settled down at the bottom of the vessel. Mechanistically, alkaline oxidation and deprotonation of cationic species were followed by dehydration resulting in black colored magnetite precipitate. Subsequently, these aggregated particles were successfully modified with organic surfactant, sodium oleate, as evident by reduction in their hydrodynamic diameter, size distribution, monodispersity and the polydispersity index (PDI) value obtained in DLS measurement (Table 1). Drastic decrease in the size of oleated modified nanoparticles can also be observed from the TEM micrographs shown in Fig 1. Oleate coating has been successfully applied on large number of nanoparticles including silver, iron, gold, carbon nanoemulsions providing higher dispersibility as compared to other common stabilizers since the repulsive force between hydrophobic surfactant molecules coated on single particles can prevent them from agglomeration.[17] Surfactant molecules form a dense protective monolayer on the surface of nanoparticles. Pretreatment of magnetite structures with oleate has several benefits apart from de-agglomeration of nanoparticles such as higher biocompatibility, improved dispersibility etc.[18]

Synthesis of PFMNCs

Free radical emulsion polymerization technique was used for the synthesis of polymer functionalized magnetic nanoconstructs with St, MMA and AAEM in the presence of different concentrations of oleate coated IONPs (3-21% w/w). Stable latexes of light to dark brown color were obtained without any phase separation indicating complete encapsulation of IONPs within

the synthesized polymeric network. Mechanistically, initial seeding of hydrophobic St and MMA along with hydrophilic AAEM create a miceller organization in aqueous medium on polymerization with SPDS as a free radical initiator. Further swelling of synthesized seeds with addition of second lot of monomers resulted in IONPs encapsulsted polymeric nanoconstructs with hydrophobic core of PS and PMMA, and hydrophilic shell of PAAEM. Iron oxide was efficiently encapsulated in the hydrophobic core of nanoconstructs due to sodium oleate modification, which makes them partially hydrophobic in nature.

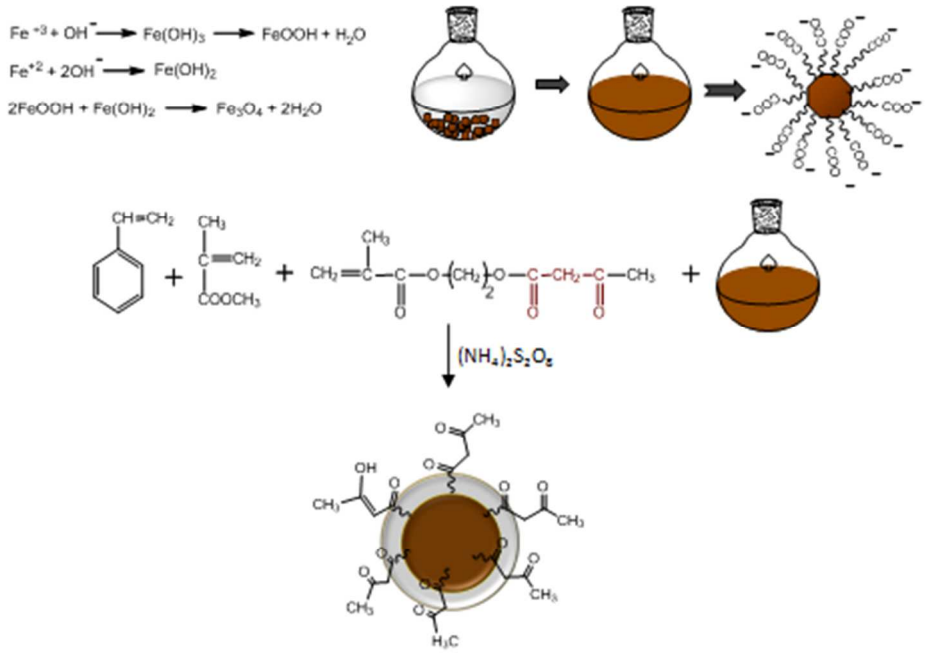

Scheme 1: Schematic representation of synthesis of iron oxide precipitate, oleate dispersion and formation of polymer functionalized magnetic nanoconstructs by emulsion polymerization

Characterization of PFMNCs

Particle size investigation by DLS (Table 1, Fig. S1) revealed that smaller particles were produced with increasing the IO content from 3 to 21% in the nanoconstruct preparation. This was attributed to increase in concentration of oleate as a surfactant in the reaction mixture, which stabilized and reduced the effective size of nanoconstructs.

Sample name	Size (diameter in nm)	PDI	Zeta potential (mV)	Antibody immobilization efficiency (%)
PFMNC-3	380	0.241	-28.7	51
PFMNC-6	299	0.125	-32.9	85
PFMNC-9	230	0.161	-33.4	82
PFMNC-12	146	0.019	-33.9	78
PFMNC-15	112	0.072	-34.6	75
PFMNC-21	101	0.082	-45.2	71

Table 1: Particle size, polydispersity index, zeta potential and antibody immobilization efficiency of various nanoconstructs

Electrokinetic properties denoted by Zeta potential (ξ) of nanostructures estimate their dispersion stability, which has significant effect on biological applications. It also revealed nature of charges present on the surface of NPs. Oleate capped IONPs showed considerable negative potential confirming substantial capping by carboxylate functionalities. A comparison of ξ of various nanoconstructs showed a higher value for PFMNCs with increased IO content (Table 1).

Modification of IONPs with polymeric system significantly improved dispersion stability, a crucial property of magnetic nanoparticle for their evaluation in biomedical applications. A very low ξ value was recorded for PFMNC-3 probably due to lesser amount of stabilizer resulting from very less IO content rendering them ineffective against external magnet. These nanoconstructs also showed least stability on storage and hence were not further characterized.

The morphology of IONPs and PFMNCs was studied by both transmission and scanning electron microscopes as shown in Fig. 1 and Fig. S2 (supplementary section). It was clearly observed that nanoconstructs were spherical in shape with regular smooth surface having monodisperse features. TEM analysis revealed the structural parameters of nanoconstructs including absolute diameters where core size was 123 nm and shell thickness was 54 nm for PFMNC-6. It could be clearly seen that PFMNCs with different IO content have regular spherical shapes showing monodispersity with uniform sizes. IONPs were effectively encapsulated within the polymeric layer and their inclusion in polymeric shell increased the core size continuously with increasing amount of IONPs from PFMNC-6 to PFMNC-21. These nanoconstructs were also easily resolved in TEM owing to strong electron density of magnetite particles. The mean diameter of PFMNCs was found to decrease with increasing IO content, which is consistent with the data obtained in DLS measurement.

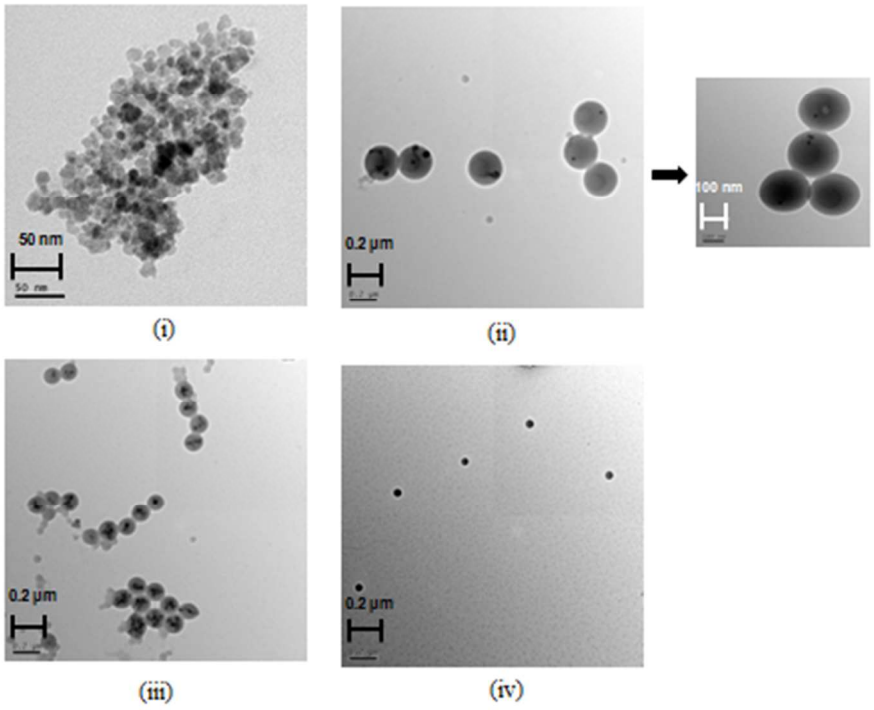

Fig. 1: TEM micrographs of (i) IONPs, (ii) PFMNC-6 along with higher magnifications, (iii) PFMNC-15 and (iv) PFMNC-21

XRD spectra of oleate capped IONPs and PFMNC-6 are presented in Fig 2. All nanoconstructs showed characteristic diffraction 2θ peaks of magnetite reflecting that the nature of iron oxide remained same, after encapsulation in polymeric nanoconstructs, without any phase change. However, to avoid overlapping of diffraction patterns, XRD of only PFMNC-6 is given in Figure 2. Sharp peaks indicate crystalline structure of IONPs. Upon encapsulation of IONPs in polymeric nanoconstructs, slight peak broadening was observed due to amorphous nature of polymeric chains. The data revealed that the characteristic peaks in PFMNCs correspond to magnetite (Fe_3O_4) and no separate amorphous domains of organic structure appeared. This result suggests that the inorganic component had effectively integrated within the polymeric network with a reasonable compatibility. The Bragg's angle 2θ = 30.1, 35.5, 43.2,53.9, 57.2 and 62.7 can be

assigned to the corresponding *hkl* values of (220), (311), (400), (422), (511) and (440) planes, respectively, of the Fe_3O_4 (JCPDS#65-3107 /821-1533). Spectral analysis indicated that IONPs and polymer modified samples have cubic spinel structure and they do not have any impurities.[19,20]

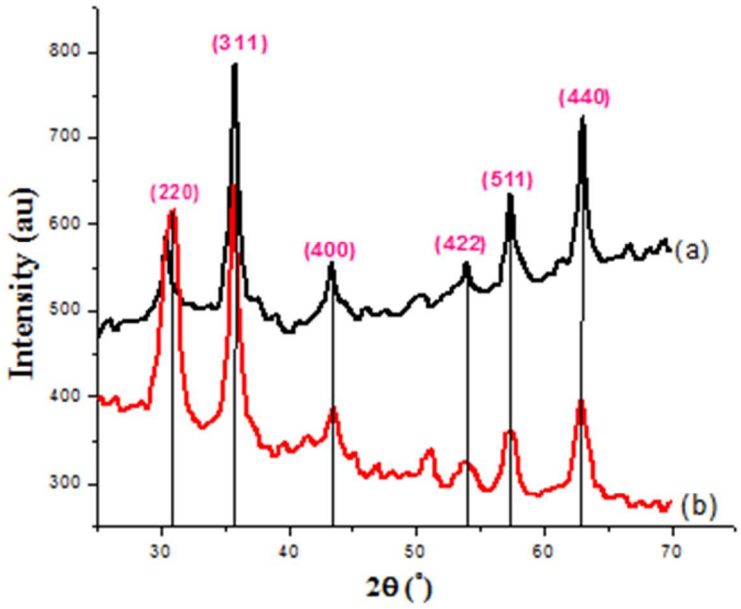

Fig 2: XRD patterns of (a) IONPs, (b) synthesized PFMNC-6

FTIR spectral analysis of unmodified and oleate modified magnetic nanoparticles was performed to confirm the presence of different functional groups generated at various reaction steps. FTIR spectra of unmodified Fe_3O_4, oleate capped IONPs and pure sodium oleate (NaOA) are shown in Fig.3. Spectrum 3(i) showed absorption peaks at 574 cm^{-1}, a shoulder peak at 587 cm^{-1} corresponding to stretching vibrations of Fe-O bond and also a small broad curve at 3348 cm^{-1} corresponding to Fe-OH stretching vibration. In Fig. 3(ii) and (iii), the strong absorptions peaks at 2920 and 2846 cm^{-1} are attributed to the asymmetric and symmetric CH_2 stretching due to aliphatic chain of oleate, respectively. In addition, bands at 1556 and 1443 cm^{-1} can be assigned to the symmetric and asymmetric stretching of the carboxylate group $\nu(COO^-)$ of the pure oleate,

respectively. δ (CH_2) scissoring band also appears in this region. In Fig 3(ii), peaks at 1556 and 1403 cm^{-1} indicate the complex formation between magnetite nanoparticles and carboxylate groups of NaOA. Carboxylic acid form complex with Fe_3O_4 in the form of monodentate, bidentate or bridges based on the difference between asymmetric and symmetric stretching vibration frequencies of carboxylate groups after coordination.[21] The spectrum shows the $\nu_{0separation}$ ($\nu_{asym}-\nu_{sym}$) of 153 cm^{-1} indicating that bidentate chelated structure was formed with Fe and two 'O' groups from NaOA. Moreover, the peak at 1703 cm^{-1} corresponding to the C=O asymmetric stretching of ester was observed in oleate capped IONPs, which confirmed the coating of iron oxide nanoparticles with sodium oleate. The observed peak broadening in the spectrum of oleate capped IONPs compared to pure oleate is due to the alignment of oleate chains on to the surface of IONPs[22].

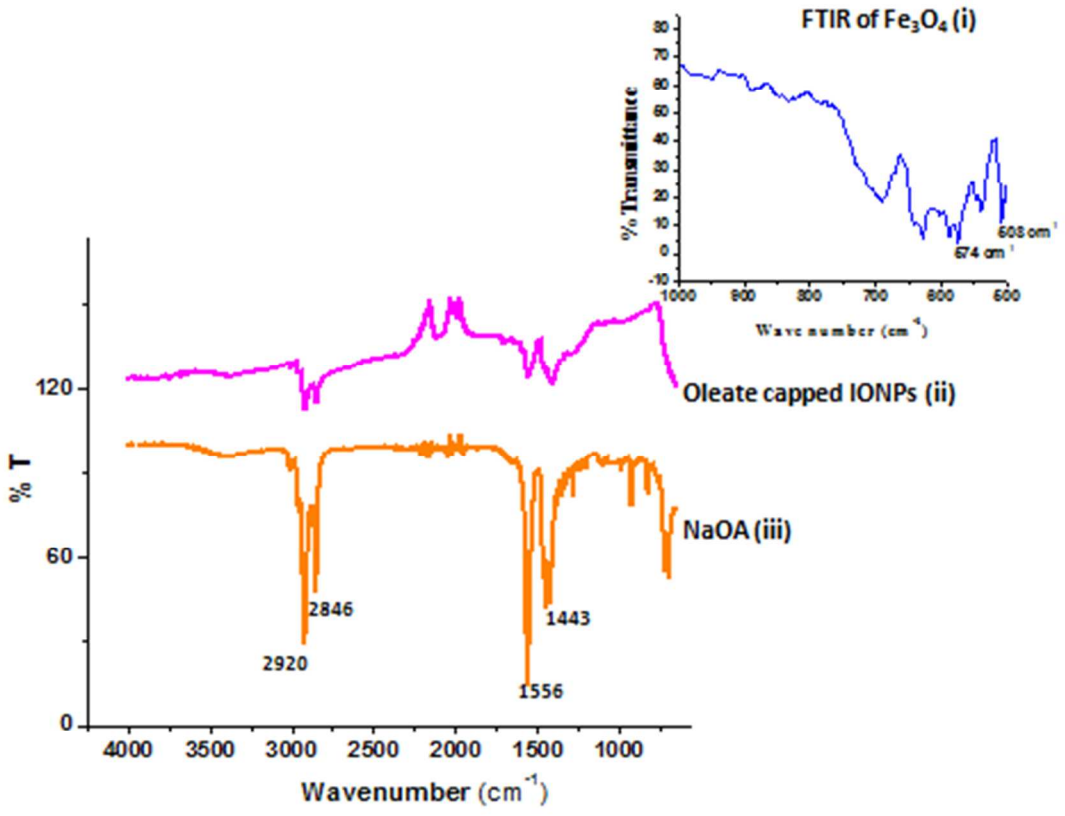

Fig 3: FTIR spectra of (i) unmodified, (ii) oleate capped IONPs and (iii) pure sodium oleate

Characteristic peak at 1638 cm^{-1} corresponding to stretching vibration of C=C of vinyl groups, disappeared in FTIR spectra of PFMNCs (Fig. 4) confirming the complete polymerization of all constituent monomers (Fig. S3 in supplementary section). It was also observed that the spectra of nanoconstructs resembled significantly with that of AAEM along with a strong band at 1725 cm^{-1} attributing to the stretching vibration of carbonyl C=O groups. PFMNCs also exhibited peaks at around 2926 and 2875 cm^{-1} as well as at 1453-1410 cm^{-1} corresponding to stretching vibration and distortion peaks of CH_2 of AAEM, respectively. This confirmed the presence of AAEM moieties primarily on the surface of nanoconstructs.

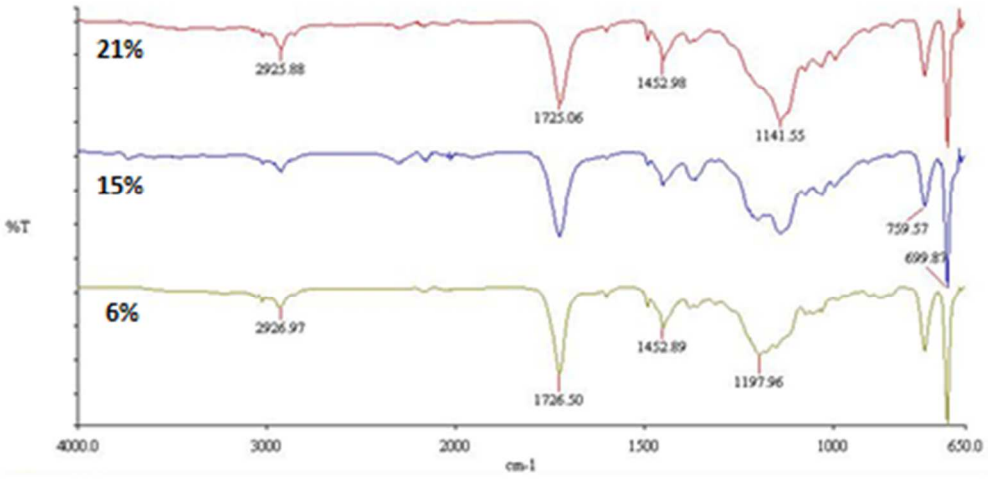

Fig. 4: FTIR spectral analysis of PFMNC-6, 15 and 21

The content of iron oxide in polymeric nanoconstructs was evaluated by thermal gravimetric analysis (TGA) and the representative graphs for PFMNCs containing 6, 15 and 21% of IONPs

are shown in Fig. 5. Complete pyrolysis of polymeric samples occurred within the tested range of temperature 100-600 °C. The data indicated that there are two step weight losses for the nanoconstructs. All the samples heated under inert atmosphere showed the first weight loss in the temperature range of 100-300°C, while the second loss occurred at 300-425°C. This thermal degradation behavior can be explained by quasi two-layer adsorbed model on particle surface.[23] The first decomposition was predominantly due to the loss of hydrogen bonded water and also for the decomposition of residual oleate from the surface of nanoconstructs. A second weight loss was because of the decomposition of polymer matrix. This weight loss during heating process was utilized for calculating the concentrations of magnetic composition in the polymer encapsulated iron oxide nanoconstructs. The weight percent of the magnetic component in the PFMNCs-6, 15 and 21 was determined to be 5.76, 14.7 and 20.8%, respectively.

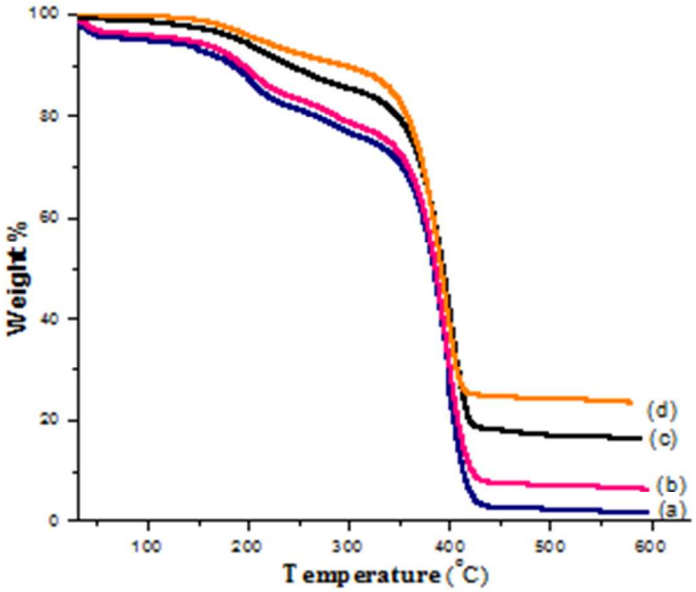

Fig. 5: TGA of PFMNCs with a) 0%, b) 6%, c) 15% and d) 21% IONPs

Magnetic character of PFMNCs was clearly confirmed from the response towards external magnetic field (Fig. S4, supplementary section), a prerequisite in immunomagnetic separation for further biosensing applications. A more detailed assessment was followed to analyze dependence of magnetism of IONPs and PFMNCs loaded with 6, 15 and 21% IONPs with applied magnetic field at 300K. All PFMNCs and IONPs exhibited superparamagnetic behavior without magnetic hysteresis. As seen in Fig. 6, the coercivity of the nanoconstructs was zero confirming their superparamagnetic properties. The magnetization curve of IONPs showed a saturation of magnetization (Ms) of 70 emu/g which is approximately 14% lower than the reported value of bulk magnetite.[24] Reduction in Ms value was observed for polymer embedded IONPs owing to thick polymeric layer. Similar observations are also reported in literature.[25-28] Although the shell layer reduced magnetic properties of the developed nanoconstructs but they showed good magnetization and also provide surface functionalities for their applications in magnetic targeting and capturing of analytes. The Ms values of 7-22 emu/g is reported to be sufficient for most of the biological applications.[29,30] Hence the amount of magnetization achieved with developed nanoconstructs is sufficient enough for the current use. It could also be easily visualized from Fig. 6 that the magnetic response to the external magnet increased with increasing amount of IONPs loading in different PFMNCs with maximum value of 23 emu/g for PFMNC-21.

No phase separation or breakage of latex was observed for the nanoconstructs which remained stable for more than a year when stored at room temperature as compared to iron oxide dispersion. Essentially naked Fe_3O_4 nanoparticles have been reported to be highly chemically labile with strong tendency for oxidation resulting in loss of magnetism and aqueous dispersibility. PFMNCs showed high dispersion stability without any change in magnetic properties on treatment with solutions of different pH for 24 hrs (data not shown). Thus, the polymeric encapsulation protects

the embedded magnetic core from various degrading environmental factors like dissolved oxygen and pH.

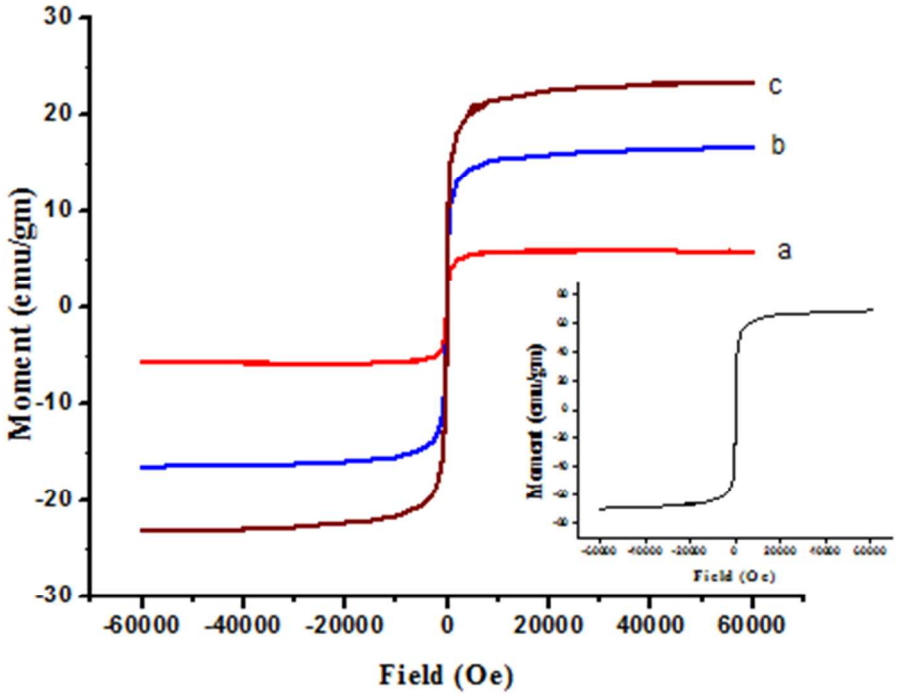

Fig. 6: M vs H hysteresis loop for different PFMNCs (a) 6, (b) 15 (c) 21 and the inset shows magnetization curve of IONPs

Immobilization of Abs

Polymeric nanoconstructs have been designed in the present work with an aim to have dual capabilities of magnetic responsiveness and surface functionalities for immobilization of biomolecules without using any linker or activator. The core of nanoconstructs created by St, MMA and IONPs is responsible for magnetic properties while surface functionalities generated by the presence of AAEM moieties to enable attachment of biomolecules. AAEM has gained popularity in recent years for biomedical applications e.g. immobilization of enzyme[31], drug delivery and for developing biomaterials.[32,33]

Antibody immobilization efficiency was calculated for all polymeric nanoconstructs conjugated with GAR-IgG using Pierce® BCA Protein assay kit. It was observed that PFMNC-6 yielded maximum immobilization efficiency (85%) as compared with other nanoconstructs (Table 1). This was attributed to the fact that nanoconstructs with higher IONPs content, have more amount of surfactant which interfere with the covalent attachment of Abs on their surface. Hence, PFMNC-6 was used for further immobilization and biosensing studies. A range of GAR-HRP conjugates were prepared by serial dilution method in 1X-PBS buffer to evaluate their efficiency of immobilization on functionalized magnetic nanoconstructs. Activity of various dilutions of enzyme conjugated antibody attached on 6% PFMNCs is presented in Fig. S5 (supplementary section). A typical sigmoidal curve was obtained depicting higher optical density at low dilution of GAR-HRP and absorbance decreased with increasing dilution from 1:2000 to 1:64000. The pattern reflected the immobilization blueprint indicating surface saturation of nanoconstructs at higher concentrations of the enzyme conjugate.

Immunomagnetic separation and colourimetric detection of antibodies

Magnetic nanoparticles play a vital role in immunomagmetic separation of biological analytes in process control steps of various applications including clinical and environmental analysis. Scheme 2 represents magnetic capture of analyte and formation of immunocomplex on the surface of synthesized polymeric nanoconstructs. Sandwich ELISA was designed on PFMNCs, where GAR-IgG was used as a primary Ab, complementary RAG-IgG as an analyte and the corresponding enzyme conjugate GAR-HRP as a detector. The analyte attached nanoconstructs (PFMNC-GAR-RAG) were easily isolated from the buffer medium by applying a strong external magnetic field, which signify the utilization of developed polymeric magnetic nanoconstructs in

various applications of purification, isolation and magnetic separation through immunological capturing and selection[34,35,36].

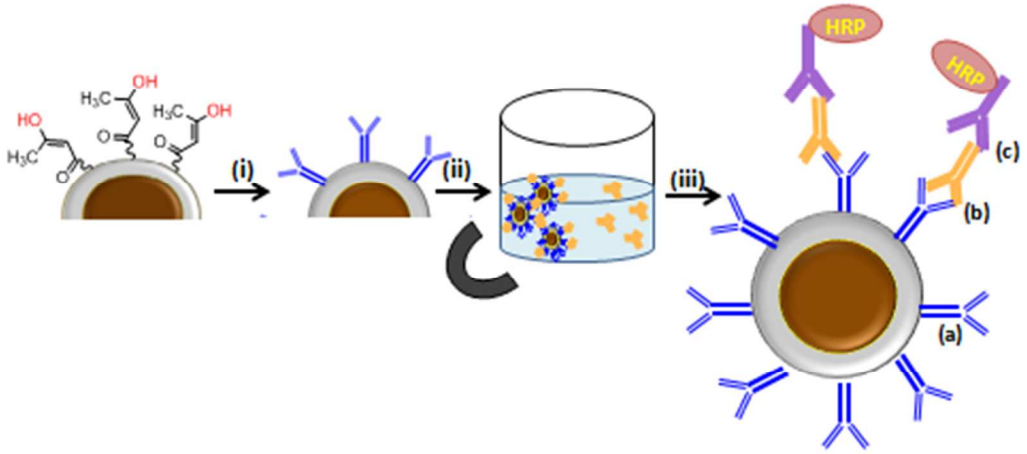

Scheme 2: Schematic representation of (i) covalent immobilization of Abs, (ii) immunomagnetic capture and (iii) detection of analyte where (a) GAR-IgG, (b) analyte RAG-IgG and (c) GAR-HRP conjugate

Optimal concentrations of individual components were statistically estimated to validate assay procedure by performing checkerboard test with varying concentrations of primary Ab and its conjugate. It was observed in Fig. 7 that with increase in dilution of the conjugate, absorbance decreased with a fixed amount of primary Ab and analyte. Subsequently, increasing concentration of attached Abs from 0.5 to 1 µg/mL resulted in more sensitive response showing higher absorbance value which is due to cumulative Ab recognition sites on the surface of nanoconstructs till a saturation point was observed. This indicated that at higher conc. (2 µg/mL onwards) saturation of primary Abs occurred due to Ab-Ab interactions and steric hindrance. Concordant results were obtained for both variables, which showed that 1µg/mL GAR IgGs and 1:4000 dilution of GAR-HRP were the optimized concentrations for further experiments. Immobilization efficiency for PFMNC-6 at this optimized concentration of GAR-IgG was determined to be 85%, which indicates higher number of attached Abs, a requisite for further capturing of analytes.

Surface diketone groups contributed by AAEM were inter-convertible with their enolic form to generate hydroxyl groups, which reacted with the amino group of lysine residue of Abs that provides a stable chemical linkage. Hence, the biomolecule attachment is favored on PFMNCs without the use of any additional crosslinker or activator such as glutaraldehyde, EDC/NHS generally used for amine or carboxylate functionality.[37] In addition, covalent attachment of biomolecules is preferred over physical absorption[38] to reduce the leaching of biological species during extensive washing which in turn results in loss of activity.

Ability of nanoconstructs for the quantitative estimation of analytes was measured in subsequent experiments. Optimized parameters were used while the concentration of RAG-IgGs was serially varied in the assay procedure. The dose response curve was acquired by assessing the absorbance against the concentration of analyte (Fig. 8). It was observed that optical density increased with increasing concentration of analyte antibody till a saturation point at 12.5 ng/mL. In lower concentration range, the absorbance enhanced linearly with monotonic rise in RAG-IgG concentration, establishing a good correlation index of R^2=0.977. The sensitivity or detection limit of the assay was found to be 0.39 ng/mL, which is statistically significant and different from that of negative control. In addition, PFMNCs not only provide large surface area and higher number of reactive sites facilitating enhance linking of primary Abs but also have higher dispersion capabilities within the analyte matrix for easier and rapid interactions of immunocomplexes.

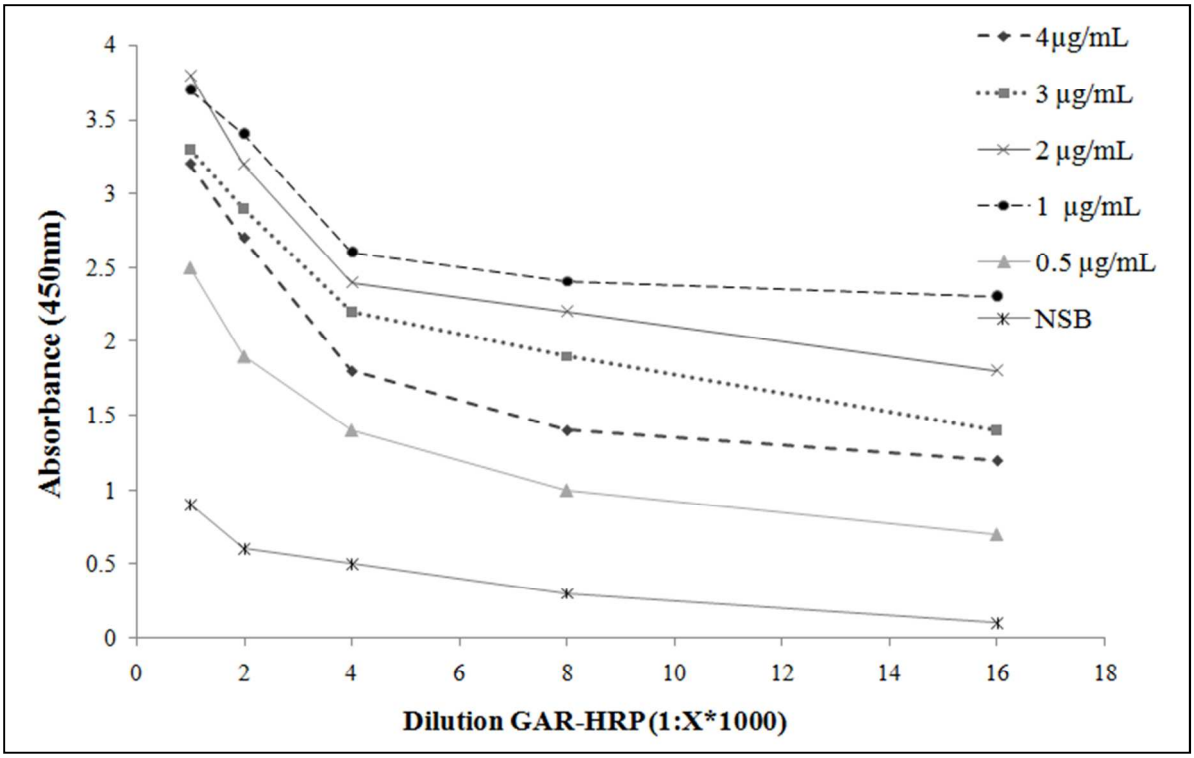

Fig. 7: Checkerboard ELISA for the optimization of parameters with the varied concentration and dilution of primary Ab and detector GAR-HRP conjugate respectively

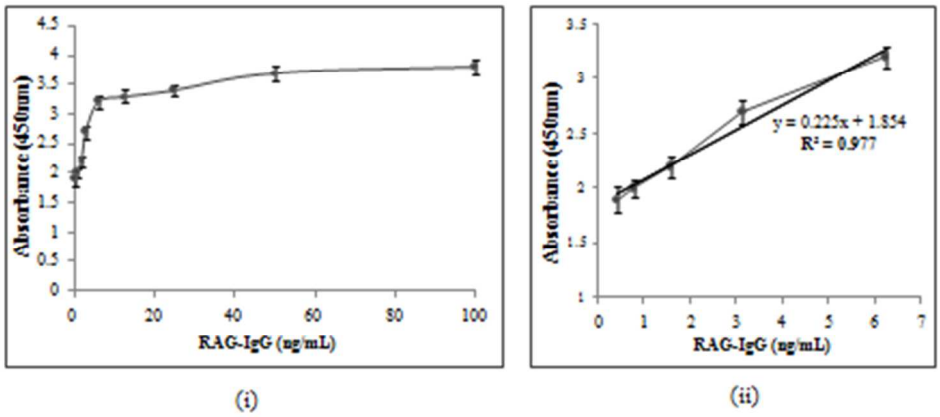

Fig 8 (i): Dose response curve of absorbance versus concentration of RAG-IgGs (ii) Optical signals depicting linear range of analyte detection with R^2=0.977

4. Conclusions

In the present work, we have reported the synthesis of a series of polymer functionalized magnetic nanoconstructs via emulsion co-polymerization of styrene, MMA and AAEM with various amounts of oleate stabilized iron oxide nanoparticles and their successful incorporation within the polymeric matrix. Morphological and FTIR analyses revealed that polymeric nanoconstructs acquired core-shell morphology with magnetic core in hydrophobic zone created by St and MMA while hydrophilic shell was constituted by AAEM. Nanoconstructs with 6% IONPs showed good aqueous dispersibility, optimal magnetic responsiveness and high Ab (GAR-IgG) immobilization efficiency. Abs were successfully covalently attached on the surface of nanoconstructs through pendant diketone functionalities without using any crosslinker or activator. The sensitivity of the sandwich ELISA assay, developed with PFMNC-6, for the detection of analyte RAG-IgG was 0.39 ng/mL with easy separation of analyte-attached nanoconstructs using external magnetic field. Thus, the developed nanoconstructs have the strong potential to be explored as an effective immunomagnetic capture and detection matrix for medical diagnostics.

Acknowledgements

Authors would like to acknowledge the financial support from Department of Biotechnology, DBT India (BT/Bio-CARe/05/9676/2013-14) for carrying out this research work.

List of schemes, figures and tables

Notes and references

1. M. Cao, Z. Li, J. Wang, W. Ge, T. Yue, R. Li, V. L. Colvin and W. W. Yu, *Trends Food Sci. Technol*., 2012, 27, 47–56.
2. M. A. M. Gijs, F. Lacharme and U. Lehmann, *Chem. Rev*., 2010, 110, 1518–1563.
3. A. H. Lu, E. L. Salabas and F. Schuth, *Chem. Int. Ed*., 2007, 46, 1222 – 1244.
4. R. Massart, *IEEE Trans. Magn*., 1981, 17, 1247-1248.
5. C. Boyer, M. R. Whittaker, V. Bulmus, J. Liu and T. P. Davis, *NPG Asia Materials*, 2010, 2, 23–30.
6. M. Chen, S. Yamamuro , D. Farrell and S. A. Majetich, *J. Appl. Phys*., 2003, 93, 7551–7553.
7. O. Philippova, A. Brabanova, V. Molchanov, A. Khokhlov, D. Suzuki and H. Kawaguchi, *Eur. Polym. J*., 2011, 47, 542–559.
8. M. A. Morales, P. V. Finotelli, J. A. H. Coaquira, M. H. M. Rocha-Leao, C. Diaz-Aguila, and E. M. Baggio-Saitovitch, *Colloid Polym. Sci*., 2006, 284, 1443–51.
9. M. A. Moralesa, P. V. Finotellia, J. A. H. Coaquirab, M. H. M. Rocha-Leãoc, C. Diaz-Aguilad, E. M. Baggio-Saitovitchb and A. M. Rossib, *Mater Sci. Eng. C*, 2008, 28, 253–257.
10. H. L. Liu, S. P. Ko, J. H. Wu, M. H. Jung, J. H. Min, J. H. Lee, B. Han and Y. K. Kim, *J. Magn. Magn. Mater.*, 2007, 310, 815–817.
11. H. Dou, B. Xu, B. Tao, M. Tang and K. Sun, *J. Mater Sci: Mater Med*., 2008, 19, 2575–2580.
12. A. Butt, A. Farrukh, C. A. Ghaffar, H. Duran, Z. Oluz, H. U. R. Rehman, T. Hussain, R. Ahmad, A. Tahir and B. Yameen, *RSC Adv.,* 2015, 5, 77682.
13. A. Zengin, E. Yildirim, U. Tamer and T. Caykara, *Analyst*, 2013, 138, 7238-7245.
14. F. Dai, M. Zhang, B. Hu, Y. Sun, Q. Tang, M. Du and X. Zhang, *RSC Adv*., 2015, 5, 3574-3580.
15. P. C. Lin, C. C. Yu, H. T. Wu, Y. W. Lu, C. L. Han, A. K. Su, Y. J. Chen and C. C. Lin, *Biomacromolecules*, 2013, 14, 160-168.
16. R. Conceição, Â. N. Moreira, R. J. Ramos, F. L. Goularte, J. B. Carvalhal and J. A. G. Aleixo, *Braz. J. Microbiol*., 2008, 39, 173–177.

17. H. Jayamohan, B. K. Gale, B. Minson, C. J. Lambert, N. Gordon and H. J. Sant, *Sensors (Basel)*, 2015, 15, 12034-12052.
18. J. Sun, S. Zhou, P. Hou, Y. Yang, J. Weng, X. Li and M. Li, *J. Biomed. Mater. Res*., 2007, 80A, 333–341.
19. A. Pich, S. Bhattacharya, A. Ghosh and H. J. P. Adler, *Polymer,* 2005, 46, 4596–4603.
20. F. Y. Cheng, C. H. Su, Y. S. Yang, C. S. Yeh, C. Y. T. Sai, C. L. Wu, M. T. Wu and D. B. Shieh, *Biomaterials*, 2005, 26, 729.
21. (a) J. Esquivel, I. A. Facundo, M. E. Trevino and R.G. Lopez, *J. Mater. Sci*., 2007, 42, 9015–9020, (b) L. M. Bronstein, X. Huang, J. Retrum, A. Schmucker, M. Pink, B. D. Stein and B. Dragnea, Chem. Mater., 2007, 19, 3624-3632.
22. G. B. Decon, Coord. *Chem. Rev*., 1980, 33, 227-250.
23. J. Wang, T. J. Shi and X. C. Jiang, *Nanoscale Res. Lett*., 2009, 4, 240–246.
24. M. Mahdavi, M. B. Ahmad, M. J. Haron, F. Namvar, B. Nadi, M. Z. A. Rahman and J. Amin, *Molecules*, 2013, 18, 7533-7548.
25. R. M. Cornell and U. Schwertmann, *VHC New York*, 2003.
26. N. A. Brusentsov, V. V. Gogosov, T. N. Brusentsova, A. V. Sergeev, N. Y. Jurchenko, A. A. Kuznetsov, O. A. Kuznetsov and L. I. Shumakov, *J. Magn. Magn. Mat.,* 2001, 225, 113–117.
27. C. J. Xu, K. M. Xu, H. W. Gu, X. F. Zhong, Z. H. Guo, R. Zheng, X. Zhang and B. Xu, *J. Am. Chem. Soc*., 2004, 126, 3392–3393.
28. M. Mahmoudi, A. Simchi, M. Imani, A. S. Milani and P. Stroeve, *J. Phys. Chem. B.,* 2008, 112, 14470.
29. S. Mohapatra, N. Pramanik, S. K. Ghosh, P. Pramanik, *J. Nanosci, Nanotechnol*., 2006, 6, 823-829.
30. P. Tartaj and C. J. Serna, *J. Am. Chem. Soc*., 2003, 125, 15754–15755.
31. A. Pich, S. Bhattacharya, H.J.P. Adler, T. Wage, A. Taubenberger, Z. Li, K. H. Pee, U. Böhmer, T. Bley, *Macromol. Biosci*., 2006, 6, 301-310.
32. V. Boyko, A. Pich, Y. Lu, S. Richter, K-F. Arndt, H-J. P. Adler, *Polymer*, 2003, 44, 7821–7827.
33. V. Delplace and J. Nicolas, *Nature Chemistry*, 2015, 7,771–784.
34. Y. J . Park, M. J. Monterio, S. V. Es and A. L. German, *Eur. Polym. J*., 2001, 37, 965-973.

35. Y. Jung, J. Y. Jeong and B. H. Chung, *Analyst*, 2008, 133, 697–701.
36. D. Brandão, S. Liébana, S. Campoy, S. Alegret and M. I. Pividori, *Talanta*, 2015, 143, 198–204.
37. P. R. Solanki, A. Kaushik, V. V. Agrawal and B. D. Malhotram, *NPG Asia Mater*., 2011, 3, 17–24.
38. S. Jain, S. Chattopadhyay, R. Jackeray, C. K. Abid and H. Singh, *Nanoscale*, 2013, 7, 6883-6892.

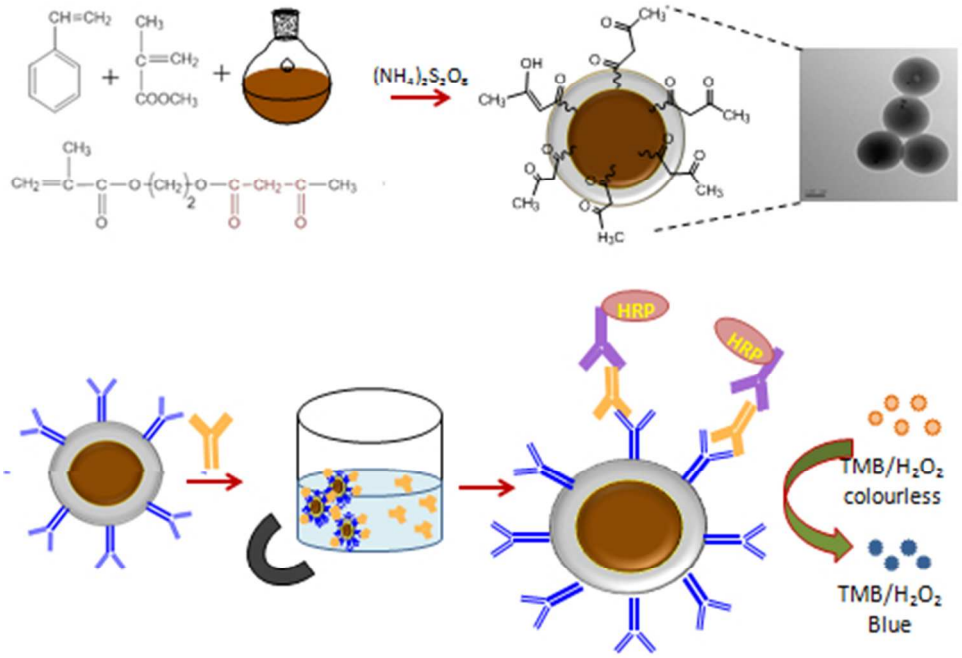

127x89mm (96 x 96 DPI)